

Hard X-ray Absorption Fine Structure Spectroscopy

De-Tong Jiang

Canadian Light Source Inc.
University of Saskatchewan

Principal Contact

Beamline Team Leader and Beamline Development Scientist	De-Tong Jiang Canadian Light Source detong.jiang@lightsource.ca
---	---

Overview

Status	Approved and funded as of December 31, 2001
Source	Superconducting 1.917-tesla 63-pole wiggler
Monochromator	Double crystal Si(111) and Si(311)
Spectral range	5–40 keV
Flux on sample	10^{13} photons/s/0.1% bandwidth at 10 keV and 0.2×0.7 mm ² spot size
Brilliance	10^{17} photons/mm ² /mrad ² / 0.1% bandwidth
Resolution ($\Delta E/E$)	10^{-4}
Focused spot size (by K-B pair)	15×8 μ m (horizontal \times vertical)

Science

X-ray absorption fine structure (XAFS) is the oscillatory structure in the X-ray absorption coefficient, measured as a function of X-ray photon energy. XAFS is usually divided into two regimes relative to the atomic absorption edge, due to differences in the data analysis. X-ray absorption near-edge structure (XANES) is the region several tens of eV above the absorption edge, whereas extended X-ray absorption fine structure (EXAFS) is the subsequent region extending up to 1000 eV above

the edge. XAFS techniques provide element-specific chemical speciation information about matter in virtually any physical state: gases, liquids, amorphous materials, or crystalline solids. XAFS analysis determines chemical bonding, valence and oxidation state, and can give quantitative data on short-range structure. Bond lengths, coordination numbers and bond disorder for each of the atomic components can be determined.

The modern understanding of XAFS was established in the early 1970s, coincident with advances in dedicated synchrotron radiation facilities. Rapid development followed, especially with the availability of more powerful third-generation light sources and better detectors. XAFS has now become an indispensable tool for fundamental and applied research in a vast range of fields. Some 25% of all synchrotron radiation beamlines worldwide are either devoted to or partially used for performing XAFS.

A major advantage of XAFS for structural determinations is that a crystalline sample is not required. This feature is particularly helpful in the geochemical sciences, catalysis studies, electrochemistry, materials science, and the environmental sciences—all fields where the samples often do not possess long-range order.

The element-specific character of XAFS provides a useful complement to methods in which the entire sample matrix contributes to the signal, such as X-ray diffraction (XRD). For example, crystal lattice constants measured by XRD typically vary linearly with composition in solid solutions (Vegard's law). This leads to the “virtual crystal approximation”, which assumes that the average atomic positions, bond lengths, and bond ionicities of alloys are the mole-weighted averages of those for the pure constituents. However, XAFS has shown that this approximation does not apply for nearest-neighbour bond lengths in binary (and some ternary) compounds. Such information allows detailed understanding and hence tailoring of the material properties in condensed matter.

The penetration power of hard X-rays permits the study of various complex systems *in situ*, including difficult cases such as supercritical solutions. Bulk samples, surfaces, or wet or buried interfaces can be studied with a surface specificity similar to conventional vacuum surface techniques, simply by geometrically confining the X-ray penetration depth (for example, by using grazing-incidence XAFS).

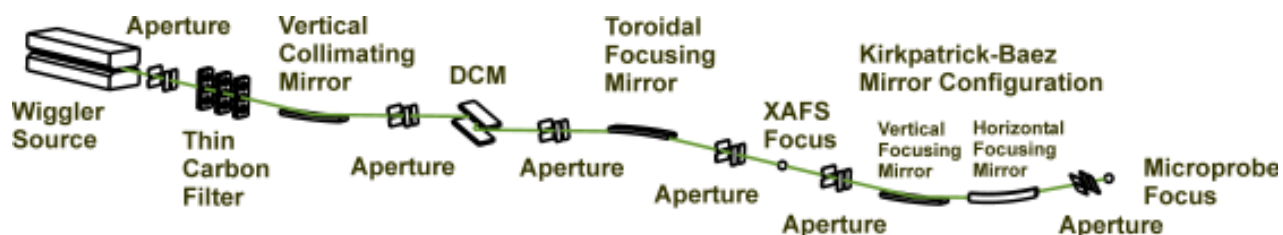


Figure 12.1 Simplified diagram of the micro-XAFS beamline.

When XAFS is combined with diffraction techniques, site- and element-specific structural characterizations become possible, enabling new methods such as diffraction anomalous fine structure (DAFS).

With the increasing maturity of these techniques, more and more industrial applications have arisen.

Instrumentation

All of the above-mentioned capabilities will be available at the CLS general-purpose micro-XAFS beamline. The primary design criterion is that the beamline must be a reliable tool for general-purpose spectroscopy. Therefore, the beamline will need a source that covers a wide range of hard X-ray photon energies, an ultra-stable beam for XAFS spectroscopy, and the maximum possible photon flux density for most common sample situations. Other aspects of the design reflect the strong emphasis placed on reliability and user friendliness, since significant use by industrial researchers is expected.

A micro-beam capability will be realized through the combination of a toroidal mirror and Kirkpatrick-Baez (K-B) mirror optics. This microprobe will be wiggler-based, and while not be as powerful as a dedicated undulator-based microprobe, it will still be of tremendous importance to the user community: this microprobe beamline is an imperative feature for the CLS.

The endstation will have the following capabilities:

- Conventional XAFS;
- Microbeam imaging and micro-XAFS;
- Powder diffraction and DAFS; and
- X-ray reflectometry.

The planned detectors include a multi-element solid-state

detector, a single-element solid-state detector, a wavelength dispersive detector, and an image plate (for powder diffraction). Sample manipulation instruments will include a two-circle diffractometer for powder diffraction and reflectometry, and micro-scanning stages.

Layout

The layout of the beamline components is given in Figure 12.1. The optics include a plane bent mirror to vertically collimate the beam from the wiggler source; a monochromator with cryogenically cooled Si (111) or Si (311) crystals; and a toroidal focusing mirror. In the experimental station, there will be a K-B mirror pair to further focus the beam for microprobe applications. When an experiment is not brilliance-limited, the sample location will be at the focus of the toroidal mirror.

Performance

The source point for the micro-XAFS beamline will be a 1.917-tesla 63-pole superconducting wiggler. The beamline is designed for high stability. It will deliver some microprobe capability over the energy range from 5 keV to 40 keV, with a resolving power of about 10 000 and competitive intensity (a flux of 10^{13} photons/sec/0.1% bandwidth).

Table 12.1 lists the machine parameters, while the wiggler parameters upon which the beamline design is based are in Table 12.2. The front-end aperture will limit the divergence of the light entering the beamline to 1.5 mrad horizontal \times 0.24 mrad vertical.

Table 12.1 Machine parameters at the centre of the straight in 2008

Horizontal beam size (σ_x)	440 μm
Vertical beam size (σ_z)	9 μm
Horizontal emittance (ϵ_x)	1.77×10^{-6} cm·rad
Vertical emittance (ϵ_z)	3.55×10^{-9} cm·rad
Ring energy	2.9 GeV
Beam current	500 mA

Table 12.2 Wiggler parameters

Magnet period (λ_u)	0.033 m
Number of magnet periods (N)	32.5
K parameter	5.91
Spectral bandwidth ($\Delta E/E$)	0.1%

Ray tracing has shown that at the focus of the toroidal mirror, the beam size will be about $0.7 \text{ mm} \times 0.2 \text{ mm}$ (horizontal \times vertical, FWHM). A Kirkpatrick-Baez (K-B) bent elliptical cylindrical mirror pair will further reduce the spot size to about $(14\text{--}19) \mu\text{m} \times (6\text{--}9) \mu\text{m}$ (horizontal \times vertical, FWHM). Figure 12.2 indicates the flux at the K-B focused spot as a function of photon energy.

Beamline Team Research Activities

XAFS of rare earth elements in hydrothermal fluids

A. J. Anderson¹, R. A. Mayanovic² and S. Jayanetti²

¹St. Francis Xavier University

²Southwest Missouri State University

Knowledge of the structure, stoichiometry and stability of rare earth elements (REEs) in hydrothermal solutions is required for a complete understanding of the distribution of REEs in the hydrosphere. We have been using XAFS to investigate the local structure of REEs dissolved in hydrothermal fluids. Lanthanum L₃-edge XAFS spectra (5480 eV) were collected from dilute (0.007 M) La- and Yb-bearing solutions in a modified hydrothermal diamond anvil cell at temperatures up to 500 °C. Results indicate that 9 oxygens surround each La ion in a tri-capped trigonal prismatic arrangement. La–OH₂ bond

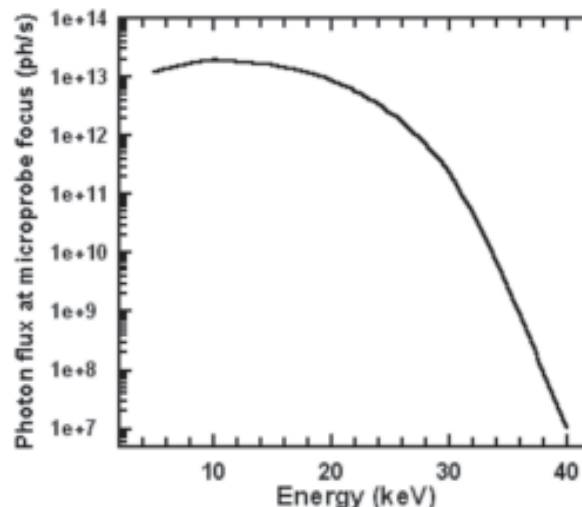


Figure 12.2 Intensity in the focused spot of the microprobe under the storage ring conditions expected in 2008. Spot size will be $(14\text{--}19) \mu\text{m} \times (6\text{--}9) \mu\text{m}$ (horizontal \times vertical, FWHM).

lengths at the equatorial plane of the trigonal prism increase with increasing temperature.

The results of our studies may provide insight into the behaviour of similar actinide group elements, which is relevant to the problem of nuclear waste storage.

This work was performed at the PNC-CAT (APS). Steve Heald, the other PNC-CAT beam line personnel, and Robert Gordon (Simon Fraser University) are all thanked for assisting with our experiments at the APS.

XAFS of magnetic Fe-Ti-O samples produced by ball milling

D.-T. Jiang¹, J. Tang² and W. Wang²

¹Canadian Light Source

²University of New Orleans

XAFS has been used to investigate the structure of a series of Fe-Ti-O magnetic semiconductors produced by ball milling iron and oxygen-reduced rutile (TiO₂). Iron K-edge XAFS measurements of the samples have been carried out using beamline 20BM at the PNC-CAT (APS). Preliminary results indicate that the room temperature ferromagnetic properties of the system may be due to an Fe-Ti-O phase in which the iron is electronically similar to that in FeTiO₃, but surrounded by rather different local structures. From the magnetic and XAFS measurements of the system, the possibility was ruled out that the magnetic properties were due to residual metallic iron.

This work was performed at the PNC-CAT (APS).

Evidence for a metal-induced conduction band in M-DNA

R. Skinner¹, Y.-F. Hu², D.-T. Jiang³, J. S. Lee¹ and R. Sammynaiken^{1,4}

¹ Department of Biochemistry, U. of Saskatchewan

² CSRF, SRC, University of Wisconsin-Madison

³ Canadian Light Source Inc., Saskatoon, SK

⁴ Saskatchewan Structural Sciences Centre, U. of S.

M-DNA is a conductor [1] formed at pH levels greater than 8.5 by replacing the imino protons of the bases in normal DNA (B-DNA) with Zn²⁺, Ni²⁺ or Co²⁺ ions [2]. Understanding the electronic structure of M-DNA will lead to an understanding of how it conducts, and will aid in developing biosensors and nanoelectronic devices.

This investigation began by using X-ray absorption spectroscopy (XAS) to probe the density of unoccupied states at several edges. At the nitrogen K edge, we observed evidence that metal ions bound to the imino nitrogen induced the formation of a conduction band.

Nitrogen 1s and nickel 2p XAS spectra were measured at the CSRF SGM beamline at the SRC. Three types of samples were prepared from sheared calf thymus DNA: (i) uncomplexed B-DNA at pH 7, (ii) a control of B-DNA and M²⁺ at pH 7, in which the metal ions were bound to the outside of the helix (metal-B-DNA), and (iii) metal-M-DNA. Complexes were prepared with three metal ions (Ni²⁺, Co²⁺, or Zn²⁺) and were dried *in vacuo*. Figure 12-3 shows a comparison of the nitrogen K-edge XANES of Ni-M-DNA, Ni-B-DNA and B-DNA. Second-order nickel L_{2,3} absorption bands were observed for both Ni-B-DNA and Ni-M-DNA.

Nickel K-edge EXAFS experiments were carried out at beamline 20BM of the PNC-CAT (APS). These results show that the nickel was in the +2 oxidation state, and that the local structure surrounding nickel in Ni-M-DNA is distinctly different from that in Ni-B-DNA. The nickel nearest neighbour shell in Ni-M-DNA appears to have two components, which could indicate two nickel coordination sites in Ni-M-DNA (for example, outside and inside the helix). In contrast, the Ni K-edge XAFS exhibits only a single first shell in B-DNA, indicating only a single type of nickel coordination site in B-DNA (for example, outside the helix). Interestingly, the nickel has a second shell signal at about 2.9 Å (non-phase-corrected distance) in both Ni-M-DNA and Ni-B-DNA.

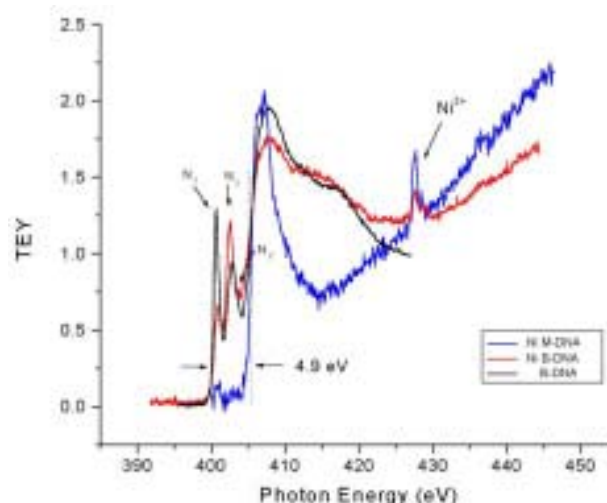


Figure 12-3 Comparison of the Ni-M-DNA, Ni-B-DNA and B-DNA nitrogen K edges, showing the collapse of discrete states and the formation of a conduction band in M-DNA.

Further analysis will be required to obtain more detailed structural interpretations of these results.

At the nitrogen K-edge, the absorption profiles of the B-DNA and the Ni-B-DNA both show the presence of discrete unoccupied states, as expected from systems that are not metal-like conductors. Assignments of these discrete states have been made by means of XANES studies on molecular nitrogen [3], and it is quite evident that there is more than one type of nitrogen [4]. On the other hand, the nitrogen K edge of the Ni-M-DNA shows a collapse in the absorption band, a 4.9 eV blue shift, and a disappearance of the discrete states. The Ni²⁺ ions bound to the imino nitrogen of the base pairs would be expected to add to the resolution of the different types of nitrogens, but instead the nitrogens become electronically indistinguishable. This is observed for all of the metal-M-DNA complexes. This suggests that upon binding with the imino nitrogen, Ni²⁺, Co²⁺, or Zn²⁺ ions induce the electronic states in the base pairs to form a conduction band. Thus, the entire M-DNA structure may behave as a conductive wire.

This work was performed at the SRC and at the APS.

References

- [1] A. Rakiktin et al. *Phys. Rev. Lett.* **2001**, 86, 3670.
- [2] P. Aich et al. *J. Mol. Biol.* **1999**, 294, 477.
- [3] C. T. Chen; Y. Ma; F. Sette. *Phys. Rev. A* **1989**, 40, 6737.
- [4] S. M. Kirtley et al. *Biochim. Biophys. Acta* **1992**, 1132, 249.

X-ray microprobe analysis of meteorites

P. A. Cavell¹, R. G. Cavell¹, P. Arboleda¹,
M. Karolewski¹ and R. Gordon²

¹ Alberta Microprobe Group, University of Alberta

² PNC-CAT, APS, Argonne, IL

Mapping elements in meteorites establishes the distribution of important trace elements such as gallium and germanium. This information can be used to classify and hence ascertain the origin of the meteorites. In addition, XANES and EXAFS data recorded using the X-ray microprobe allowed the determination of the chemical speciation of these trace elements, information hitherto unavailable for such materials. The distributions of iron and gallium in an area containing at least two iron-nickel minerals are mapped in Figure 12·4 and Figure 12·5. These maps (as well as others of the germanium and nickel distributions) were obtained using the PNC-CAT ID microprobe (APS Sector 20), focused to an excitation spot approximately 5 micrometres in diameter.

Fluorescent X-ray signals were collected using a 13-element solid-state detector. XANES and EXAFS analyses at various points indicated that each element occurred in different oxidation states and occupied different chemical environments in each area of the sample. This information will provide more a detailed understanding of the origin of meteorites.

The data sets for this work were collected at the APS.



Project Leader and Acting Executive Director Mark de Jong explains the CLS accelerator structures to Finance Minister Paul Martin, U. of Saskatchewan President Peter MacKinnon, and U. of S. V.P. (Finance and Resources) Tony Whitworth.

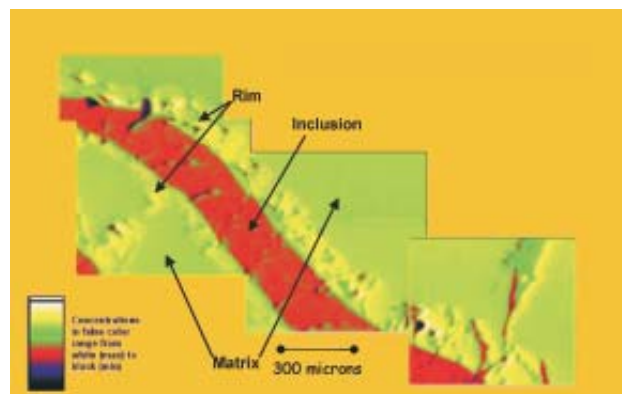


Figure 12·4 Map of the distribution of iron in a selected area of the Canyon Diablo meteorite.

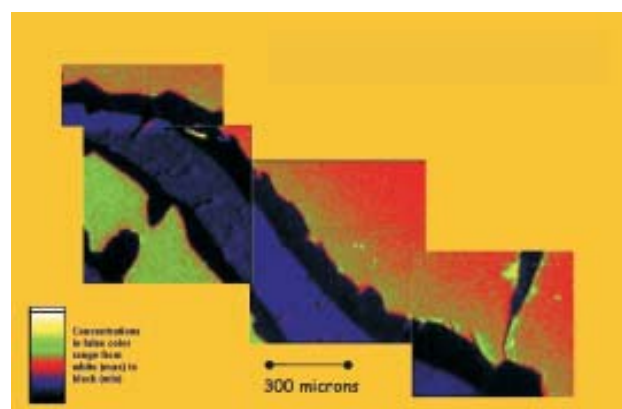


Figure 12·5 Map of the distribution of gallium in a selected area of the Canyon Diablo meteorite.

Beamline Design and Beamline Team

Table 12·3 lists the beamline design team, which established the endstation and beamline properties. Table 12·4 lists Canadian scientists active in XAFS or microprobe studies, and who are team members or potential users. Table 12·5 gives the milestones for the beamline project. 🌟

Table 12·3 XAFS beamline design team

Canadian Light Source	De-Tong Jiang Weifan Sheng Ingvar Blomqvist Emil Hallin
University of Alberta	Ron Cavell
Stacie Institute for Molecular Sciences (NRC)	John Tse Dennis D. Klug
University of Ottawa	Serge Desgreniers

Table 12-4 Beamline team and future users

Canadian Light Source and University of Saskatchewan	De-Tong Jiang Jeff Cutler Jim Hendry Yuanming Pan
INRS, QC	Daniel Guay Jean-Claude Kieffer
McGill University	Don Baker
University of Guelph	Jacek Lipkowski
St. Francis Xavier University	Alan Anderson
Steele Institute for Molecular Sciences, NRC, ON	John S. Tse Dennis D. Klug C. Paul
University of Ottawa	Serge Desgreniers S. Scott
NRCan, ON	Jim Brown Jeanne Percival
University of Alberta	Ron Cavell P. A. Cavell Marcus Karolewski R. W. Luth A. Woodland
University of Toronto	Grant S. Hendersen R. J. D. Miller
University of Western Ontario	G. Michael Bancroft M. Fleet M. Kasrai N. S. McIntyre T. K. Sham M. J. Stillman
Dalhousie University	Jeff Dahn
St. Mary's University	Marc Lamoureux
Brandon University	Xiaoqian (Sam) Yan
Cameco Corporation, SK & ON	Brett Moldovan P. G. Landine E. Ozberk J. R. Mycroft
COGEMA Resources Inc., SK	N. Chen
NEC Moli Energy (Canada) Limited, BC	J. N. Reimers
Teck Cominco Limited, BC	P. Zielinski
Air Force Research Laboratory Wright-Patterson AFB, OH	J. Zabinski J. Sanders



Accelerator physicist Jack Bergstrom with Rhonda Lenton in the CLS entrance hall.

Table 12-5 Milestones for beamline development

March, 2002	Preliminary design
April, 2002	External review report
January, 2004	Commissioning